AFRL-RX-WP-TP-2010-4064

AUTOMATED IDENTIFICATION AND CHARACTERIZATION OF SECONDARY & TERTIARY γ' PRECIPITATES IN NICKEL-BASED SUPERALLOYS (PREPRINT)

M.A. Tschopp

Mississippi State University

J.S. Tiley and G.B. Viswanathan

Metals Branch
Metals, Ceramics & NDE Division

JANUARY 2010

AIR FORCE RESEARCH LABORATORY
MATERIALS AND MANUFACTURING DIRECTORATE
WRIGHT-PATTERSON AIR FORCE BASE, OH 45433-7750
AIR FORCE MATERIEL COMMAND
UNITED STATES AIR FORCE

REPORT DOCUMENTATION PAGE

Form Approved
OMB No. 0704-0188

1. REPORT DATE *(DD-MM-YY)*	2. REPORT TYPE	3. DATES COVERED *(From - To)*
January 2010	Journal Article Preprint	01 January 2010 – 01 January 2010

4. TITLE AND SUBTITLE

AUTOMATED IDENTIFICATION AND CHARACTERIZATION OF SECONDARY & TERTIARY γ' PRECIPITATES IN NICKEL-BASED SUPERALLOYS (PREPRINT)

5a. CONTRACT NUMBER
In-house

5b. GRANT NUMBER

5c. PROGRAM ELEMENT NUMBER
62102F

6. AUTHOR(S)

M.A. Tschopp (Mississippi State University)
J.S. Tiley and G.B. Viswanathan (AFRL/RXLM)

5d. PROJECT NUMBER
4347

5e. TASK NUMBER
RG

5f. WORK UNIT NUMBER
M02R1000

7. PERFORMING ORGANIZATION NAME(S) AND ADDRESS(ES)

Mississippi State University
Center for Advanced Vehicular Systems
Starkville, MS 39762

Metals Branch (AFRL/RXLM)
Metals, Ceramics & NDE Division
Materials and Manufacturing Directorate
WPAFB, OH 45433-7750
Air Force Materiel Command, United States Air Force

8. PERFORMING ORGANIZATION REPORT NUMBER
AFRL-RX-WP-TP-2010-4064

9. SPONSORING/MONITORING AGENCY NAME(S) AND ADDRESS(ES)

Air Force Research Laboratory
Materials and Manufacturing Directorate
Wright-Patterson Air Force Base, OH 45433-7750
Air Force Materiel Command
United States Air Force

10. SPONSORING/MONITORING AGENCY ACRONYM(S)
AFRL/RXLMD

11. SPONSORING/MONITORING AGENCY REPORT NUMBER(S)
AFRL-RX-WP-TP-2010-4064

12. DISTRIBUTION/AVAILABILITY STATEMENT
Approved for public release; distribution unlimited.

13. SUPPLEMENTARY NOTES
Journal article submitted to Materials Science and Technology. PAO Case Number: 88ABW-2009-3970; Clearance Date: 14 Sep 2009. Paper contains color.

14. ABSTRACT

The use of different electron loss edges in energy filtered transmission electron microscopy (EFTEM) has allowed researchers to capture images of the morphology and size of precipitates in nickel-based superalloys. In this work, we discuss a computational methodology for automated detection of secondary and tertiary γ' precipitates in EFTEM images. The optimum parameters for the automated region growing technique were identified using a combination of visual inspection and intensity information from the EFTEM images. The microstructural statistics obtained from the segmented γ' precipitates agreed with those of the manually segmented precipitates. Then, automated segmented precipitates are used to extract microstructural information about the distributions of equivalent diameters of 656 tertiary precipitates along with the distances to the nearest secondary precipitates. The significance of this technique is its ability to automate segmentation of precipitates in a reproducible manner for acquiring microstructural statistics that relate to both processing and properties.

15. SUBJECT TERMS
energy filtered transmission electron microscopy, EFTEM, automated detection, nickel-based superalloy, characterization

16. SECURITY CLASSIFICATION OF:			17. LIMITATION OF ABSTRACT:	18. NUMBER OF PAGES	19a. NAME OF RESPONSIBLE PERSON (Monitor)
a. REPORT	b. ABSTRACT	c. THIS PAGE			Christopher F. Woodward
Unclassified	Unclassified	Unclassified	SAR	32	19b. TELEPHONE NUMBER *(Include Area Code)* N/A

Standard Form 298 (Rev. 8-98)
Prescribed by ANSI Std. Z39-18

Automated Identification and Characterization of Secondary & Tertiary γ' Precipitates in Nickel-based Superalloys

M.A. Tschopp[a,b], J.S. Tiley[a], G.B. Viswanathan[a]

[a] Air Force Research Laboratory, Materials and Manufacturing Directorate, AFRL/RX
Wright Patterson AFB, OH 45433

[b] Center for Advanced Vehicular Systems
Mississippi State University, Starkville, MS 39762

The use of different electron loss edges in energy filtered transmission electron microscopy (EFTEM) has allowed researchers to capture images of the morphology and size of precipitates in nickel-based superalloys. In this work, we discuss a computational methodology for automated detection of secondary and tertiary γ' precipitates in EFTEM images. The optimum parameters for the automated region growing technique were identified using a combination of visual inspection and intensity information from the EFTEM images. The microstructural statistics obtained from the segmented γ' precipitates agreed with those of the manually segmented precipitates. Then, automated segmented precipitates are used to extract microstructural information about the distributions of equivalent diameters of 656 tertiary precipitates along with the distances to the nearest secondary precipitates. The significance of this technique is its ability to automate segmentation of precipitates in a reproducible manner for acquiring microstructural statistics that relate to both processing and properties.

KEYWORDS: energy filtered transmission electron microscopy; EFTEM; automated detection; nickel-based superalloy; characterization

1. INTRODUCTION

The underlying γ' precipitate structure in nickel-based superalloys plays a commanding role in the mechanical behavior of these alloys at high temperatures [1-3]. Previous work [4, 5] has shown that changes in processing can result in large changes in high temperature mechanical properties, such as creep and fatigue. Therefore, it is vital to be able to characterize the statistics related to γ' precipitates in these alloys to assess how influence of various processing conditions. Previous work by some of the present authors has shown that the use of automated image processing techniques are helpful in segmenting microstructure features that drive many of the strengthening mechanisms in titanium and nickel base super alloys [6-8]. Additionally, Tiley *et al.* [6] and others [9, 10] have shown that energy filtered transmission electron microscopy (EFTEM) is the state of the art technique for imaging γ' precipitates.

While much effort has been expended to refine techniques for imaging γ' precipitates in EFTEM images, the analysis of these images is also very important and in many cases can be the bottleneck of the process. Manual identification of the precipitate structure is very time-intensive and may not be reproducible between researchers. Automating the segmentation process for secondary and tertiary γ' precipitates is required to accurately compare the influence of processing on the underlying γ' structure. Reliable assessment of microstructural statistics related to the precipitate size distributions and distances between precipitates is critical for models that predict precipitate microstructure evolution and mechanical properties.

In this paper, we present an *automated* technique for detecting secondary and tertiary γ' precipitates in EFTEM images of nickel-based superalloys. The first section briefly describes the processing history for the nickel-based superalloy and the acquisition process for the EFTEM images. The second section describes the automated technique used to identify the γ' precipitates. The third section then examines and optimizes several key parameters used in the automated technique. Last, the fourth section uses this automated technique to segment the secondary and tertiary γ' precipitates in eight EFTEM images and calculates the associated microstructural statistics. The significance of this technique is its ability to automate

segmentation of precipitates in a reproducible manner for acquiring microstructural statistics that relate to both processing and properties.

2. EXPERIMENTAL METHODOLOGY

A nickel-based superalloy sample (Rene88DT) was cut from a forged disc developed under a Defense Advanced Research Projects Agency funded effort [11]. The sample was solutionized at 1050° C to dissolve primary γ' and then water quenched and subsequently aged at 760°C for 25 hours to produce a fine dispersion of uni-modal γ' precipitates. From earlier work, it is known that the Co and Cr preferentially segregate to the matrix material [6]. The Al, Nb, Ti, and Ni elements segregate to the ordered γ'. Samples were cut and polished to produce TEM foils with a 50-nm thickness. The samples were imaged on a Technai FEI 200-kV TEM using a Gatan Imaging Filter. Previous work found that the Chromium edge in EFTEM images provided the best gamma prime precipitate contrast for quantifying precipitate sizes and area fractions [12]. In contrast to that work, this work uses 30 precipitates from Cr edge EFTEM images to find the optimum parameters for an automated segmentation technique.

Figure 1 shows images of eight secondary (1-8) and eight tertiary (9-16) γ' precipitates extracted from EFTEM images that were slow cooled. Several problems with segmenting the γ' precipitates are apparent from Figure 1, *e.g.*, the morphology of the secondary precipitates, the changes in intensity within the precipitates, the intensity gradient at the boundaries, and a low level of noise. Some of the intensity changes within the secondary precipitates are typically due to a low volume fraction of the precipitate within the thin film, *i.e.*, during preparation, the TEM foil barely sliced through the precipitate in some locations (*e.g.*, the upper right corner of the precipitate in image 3). While the tertiary precipitates are all spherical in shape, the particles selected included some precipitates that would be difficult to manually segment (*e.g.*, image 15) and even some overlapping particles (*e.g.*, image 16).

[INSERT FIGURE 1 HERE]

3. AUTOMATED SEGMENTATION METHODOLOGY

While classical image processing techniques [13, 14] for segmenting image data have certain advantages, there are some limitations of using these techniques as well. For instance, a classical approach to image processing consists of two steps [15]: (1) an enhancement step, in which the intensity difference between the features of interest and the background are amplified through the application of filters and transforms, and (2) a segmentation step, in which the features of interest are extracted from the subsequent image. As Simmons and colleagues [15] point out, it is unrealistic to expect one segmentation technique to work on the vast number of materials microstructures. Here, we have used the region growing technique to segment the γ' precipitates. Region growing algorithms are widely used in medical imaging applications [*e.g.*, 16-18] and should have the ability to even segment γ' precipitates in EFTEM images with poor contrast.

Region growing is a fundamental segmentation technique in image processing [13, 14]. The basic procedure for region growing is to start with a "seed" point and grow the region by adding neighboring pixels that have properties similar to the seed (*e.g.*, similar intensity). The region grows based on a similarity criteria and stops growth when no more neighboring pixels satisfy this criteria. For example, the growth criterion is often based on the intensity difference between the neighboring pixel and the average intensity of the region. For this example, a threshold parameter can be used for the stopping criterion; when the intensity difference for all neighboring pixels is above this threshold, growth of the region stops. This "naïve" method can be used to segment the γ' precipitates, but with a few disadvantages:

1. The perimeter of the segmented particle can be very rough due to inherent noise within the image. In reality, though, the surface energy of the γ' precipitates will act to minimize the region perimeter. While median or Gaussian filters can be used to reduce the noise within the EFTEM images, these methods will also blur the edges of the particle, making it difficult to accurately segment the particle boundaries.
2. The threshold parameter used for a stopping criterion may need to be changed to accurately segment different particles. Additionally, this threshold parameter may not be obvious based on visual observation of the region boundary, *i.e.*, the precipitate interface

has a gradual intensity slope and multiple threshold parameters may appear to approximate the region boundary.

We addressed these disadvantages to create a fully automated region growing technique for segmenting the γ' precipitates. First, to discourage non-spherical growth with the region growing technique, the addition process was modified to include a weighting factor that is a function of the local density of region pixels. To implement this, the intensity difference is calculated for each pixel neighboring the region. However, instead of adding the pixel with the closest intensity value, the intensity difference for each pixel is multiplied by a weighting factor function and the pixel with the lowest value is added. In this research, the weighting factor function is given by

$$w(n) = \text{ceil}\left(\frac{e^c}{e^n}\right),$$

where n is the number of neighbors belonging to the region in a local neighborhood centered around each pixel and the constant c normalizes the weighting function so that the value of $w(c) = 1$. The ceiling function is used so that only pixels with a number of neighbors below c are adversely weighted. By multiplying this weighting function by the intensity difference for each pixel, this places a lower probability of adding a pixel surrounded by a small number of pixels belonging to the region.

Second, the stopping criterion of the "naïve" region growing was automated to select a threshold parameter for each precipitate in an unsupervised manner. This is accomplished by incrementally increasing the threshold parameter for the region growing algorithm and finding the threshold parameter that maximizes a penalty function. In this work, the penalty function is the intensity difference between mean intensities from the "inner" and "outer" regions. For instance, the "inner" region can represent all pixels within the region and the "outer" region can represent the bordering pixels just outside the region. The critical threshold parameter maximizes the penalty function and results in the optimum segmentation for the precipitate.

Figure 2 illustrates how the automated stopping criterion works for a typical γ' precipitate. First, Figure 2(a) shows the region size (pixels) as a function of the threshold parameter selected for a seed point within the γ' precipitate. The size of the region increases as the threshold parameter increases, as shown in the accompanying images (where the perimeter pixels for the segmented γ' precipitate is shown in red on the original image). After a period of fast growth to the boundary, further increases in the threshold parameter result in only minor increases to the region size. This illustrates the difficulty with choosing a threshold parameter based on visual observation alone. With only minimal changes to the region size for higher threshold parameters, at what threshold is the particle accurately segmented?

[INSERT FIGURE 2 HERE]

To answer this question, Figure 2(b) shows the mean intensity of the region, the mean intensity of the neighboring pixels, and the intensity difference between these two areas as a function of the threshold parameter for the same γ' precipitate. Recall that the maximum intensity difference (red) is the stopping criterion. For small threshold parameters, the intensity of the area outside the region is approximately equivalent to the intensity of the area inside the region, *i.e.*, many of the pixels outside the region belong to the γ' precipitate. The abrupt increase in the intensity difference coincides with the region growing near the precipitate interface, as can be seen in Figure 3(a). Again, recall that the optimum segmentation of the γ' precipitate is defined as the threshold parameter that yields the maximum intensity difference between these two areas, as denoted by the red arrow. In this automated manner, this routine quantitatively delineates the γ' precipitate interface based on the intensity gradient across the interface. The image in Figure 3(b) shows the original image with the perimeter pixels for the segmented γ' precipitate in red.

There are several potential parameters that could be used to tune the results of the region growing algorithm. For instance, the calculation of the intensity difference requires a border width (pixels) used for calculating the mean intensity of the outer region. Additionally, the calculation of the region's mean intensity can use pixels from the entire region or just pixels from the outer border of the region. Moreover, the local density weighting function contains two parameters: the constant c and the size of the local neighborhood (m x m). These parameters will

be investigated in the next section. A combination of both visual inspection and quantitative comparison of the intensity difference for different segmented particles will be used to find the optimum parameters for segmenting secondary and tertiary γ' precipitates from EFTEM images.

4. SEGMENTATION OPTIMIZATION RESULTS

4.1 Influence of intensity difference calculation

The first parameter that was investigated was the width of the border just outside the region. Multiple gamma prime precipitates were segmented using seven different widths (in pixels): 1, 2, 3, 4, 5, 6, and 7. Additionally, the mean intensity of the region was calculated using (i) the entire region and (ii) the outer boundary layer of the region. For these calculations, the values of the local density weighting function parameters were $c = 9$ and $m = 5$. Figure 3 shows an example of how these factors influence the particle segmentation. For the sake of brevity, only two different widths are used along with the two methods used for calculating the region mean intensity. The numbers '2' and '7' refer to the border width in pixels, while the letters 'i' and 'ii' refer to the method for calculating the region mean intensity. From Figure 3, a few trends are apparent through visual observation and supporting quantitative results:

[INSERT FIGURE 3 HERE]

1. As the width of the border used for the mean intensity outside the region is increased, the segmented precipitate size decreases. However, this trend is drastically reduced or eliminated by using method 'ii' (the inner border) to calculate the region intensity.
2. For method 'i', which uses the entire region to calculate the inner mean intensity, the stopping criterion misses the precipitate interface and allows the region to grow into the surrounding area, as evident in cases 2i and 7i. Additionally, this method does an inadequate job of capturing certain geometric features in the primary γ' precipitates (shown by red arrows).
3. For method 'ii', which uses the outer boundary layer of the region to calculate the inner mean intensity, the stopping criterion appears to work well.

Based on these findings, method 'ii' is the optimum method for segmentation of the precipitates in this study. The width of the border has less of an influence for this method, so a width of 7 pixels will be used as the optimum border width parameter.

4.2 Influence of local density weighting function parameters

The second parameter investigated was the influence of the local density weighting function. The optimum border width and method for calculating the intensity difference from Section 4.1 was used for this study. All 30 γ' precipitates were segmented using different values of *m* and *c*, which are listed in Table 1. Recall that *c* normalizes the weighting function, so that a density of region pixels equal to or greater than *c* within the *m* x *m* local neighborhood is not adversely weighted. Therefore, the parameter value of *m/c* = 3/1 does not adversely weight any pixels (*i.e.*, the local density weighting function does not influence the region growing technique, $w(n) = 1$ for all pixels). Table 1 lists the average percentage change (rounded to the nearest percent) in area and perimeter for the 15 secondary and 15 tertiary γ' precipitates for the *m/c* parameter combinations. The percentage change in area and perimeter is calculated by comparing the statistics for the *m/c* combination of each precipitate with those of the *m/c* = 3/1 combination. The weighting function parameters have little effect on the precipitate area, but a large effect on the perimeter measurement for the γ' precipitates. The precipitate perimeter decreases as *c* is increased for a fixed neighborhood size (*m*).

[INSERT TABLE 1 HERE]

Figure 4 illustrates how the *m/c* parameters influence the segmentation of a tertiary γ' precipitate. The perimeter of the segmented region is shown by red pixels on the original intensity image. First, the region starts to grow in a faceted manner as m/c^2 approaches 0.5 (images at the far right in Figure 4). This growth is due to the region growing algorithm adversely weighting all pixels that do not have at least 50% of their pixels in a local neighborhood, *i.e.*, the growth is dominated more by local density of region pixels than the intensity of the added pixels. This type of growth is inadequate for capturing the morphology of the precipitates. Moreover, for low values of c, the region can grow in a fingering manner with a jagged interface (*i.e.*, low percentage change in

the perimeter lengths in Table 1). Therefore, a high value of c is ideal for growing a region with a smooth interface (compared to low *c* values) as long as faceted growth is avoided. From this analysis, the optimum parameters for region growing are *m/c* values of 5/9 or 7/21.

[INSERT FIGURE 4 HERE]

4.3 Influence of initial seed location

The third area to be investigated is the initial location of the seed point. In the previous examples, the lowest intensity (darkest) pixel within the precipitate was selected as the seed point. Based on the initial segmentation using the lowest intensity pixel, 250 random pixels within the precipitate were selected as starting seed points. The optimum parameters from Sections 4.1 and 4.2 were used for this study. After all 250 regions were grown, the statistics were analyzed.

Figure 5 shows all of the random seed points on the original intensity image. The color of the seed points denote the area of the region grown from that seed relative to the area of the region grown from the lowest intensity pixel. Of the 250 regions, 191 of the regions were equal to (red), 38 were less than (green), and 21 were greater than (blue) the region grown using the lowest intensity seed point. The spatial location and intensity of the seed point made a difference in the final segmented region. First, seed points selected on the exterior of the precipitate have an increased chance of deviating from the segmentation produced using interior seed points. This effect is mainly influenced by the intensity difference in the interface region. For example, the region in the lower right of the precipitate in Figure 5 has a higher mean intensity (lighter) than the rest of the precipitate and is closer to the intensity of the surrounding matrix. Therefore, many of the seed points within this region had a higher or lower region area than seed points selected in the darker regions of the precipitate. Based on these findings, seed points that accentuate the intensity difference between the precipitate and the matrix should be selected for the region growing technique, *i.e.*, the darkest pixel in a dark particle or the lightest pixel in a light particle.

[INSERT FIGURE 5 HERE]

4.3 Validation

Using the optimum parameters outlined in Sections 4.1, 4.2, and 4.3, the initial precipitates were segmented using the region growing algorithm. Figure 6 shows the original precipitates from Figure 1 with the perimeter of the segmented region shown by the red pixels. For both the secondary and tertiary γ' precipitates, a visual comparison of the segmented regions with the intensity images shows good agreement. The region growing technique was even adequate at segmenting some of the more difficult precipitates, *e.g.*, secondary precipitates with complex morphologies (1, 3, 4, 5, & 6) and a high intensity contrast within the precipitate (3 & 5) as well as tertiary precipitates that had very diffuse interfaces with intensities very near to the surrounding matrix (14, 15, & 16).

[INSERT FIGURE 6 HERE]

Additionally, 50 secondary and tertiary γ' precipitates were selected to compare the difference between manual and automated segmentation. All of the particles were segmented using the region growing technique with the optimum parameters. The results are shown in Figure 7, which plots the area obtained via manual segmentation against the area obtained via the region growing technique. The 45° line indicates a 1:1 correlation of the areas. The areas found with the region growing technique are, on average, 14% smaller than those same precipitates segmented manually (*i.e.*, 7% smaller equivalent diameter). The inlaid images show several secondary and tertiary γ' precipitates along with the perimeter of precipitates identified with manual (blue) and automated (red) segmentation techniques. In this instance, manual segmentation tended to capture very light intensity differences in the interface region between the γ' precipitate and the γ matrix. However, in some cases, this method may actually capture some of the γ matrix pixels as well. Moreover, the results obtained using manual segmentation are highly user-dependent. In contrast to the manual segmentation, the automated region growing technique captures the precipitate and its interface based on a quantitative metric (the

intensity difference) in a reproducible manner. In the event that the region growing technique should be tuned to the manual segmentation, the penalty function can be modified.

[INSERT FIGURE 7 HERE]

5. PRECIPITATE STATISTICS RESULTS

The secondary and tertiary γ' precipitates can now be segmented using the automated region growing technique to extract microstructural statistics from the EFTEM images. Eight EFTEM images from a sample that was slow cooled after aging for 200 hours were examined because of the presence of both secondary and tertiary γ' precipitates within the microstructure. Figure 8(a) shows an example of one of the original intensity EFTEM images with the perimeters of the segmented secondary and tertiary γ' precipitates in blue and red, respectively. A number of microstructural statistics (*e.g.*, area, equivalent diameter, perimeter, etc.) can now be extracted from the segmented precipitates. Figure 8(b) shows an example of the distribution of equivalent diameters (nm) for the 656 tertiary γ' precipitates segmented from these images. The equivalent diameter for the tertiary γ' precipitates was chosen as an example statistic, because most of the tertiary γ' precipitates are spherical for this processing condition (unlike the secondary γ' precipitates). On average, the tertiary γ' precipitates have an equivalent diameter of 26 nm and the distribution is lognormal. For this microstructure, the secondary γ' precipitate statistics are not easy obtained since unconnected segments of secondary γ' precipitates within the EFTEM image can actually be part of the same secondary precipitate. Several examples of this can be observed within Figure 8(a). Therefore, a distribution of equivalent diameter for the secondary precipitates is not shown here; care should be used when using 2D statistics to describe 3D precipitates of complex morphology.

[INSERT FIGURE 8 HERE]

Another characteristic statistic that can be directly tied to the processing history of the microstructure is the nearest neighbor distances between precipitates. Again, the nearest neighbor distances between secondary γ' precipitates from 2D images are skewed in that they

may not represent the closest distance between precipitates, but rather the closest distance between branches of the same precipitate (see Figure 8(a)). Of particular interest is the nearest neighbor distance between the secondary and tertiary γ' precipitates. For each tertiary γ' precipitate, the distance to the nearest secondary γ' precipitate was calculated. Here, the distance is calculated as the minimum distance from the segmented boundary of the tertiary precipitate to the boundary of the secondary precipitate. Figure 9 shows the distribution of nearest neighbor distances for the 656 tertiary γ' precipitates. The average nearest neighbor distance was 94 nm. Taking into account the average equivalent diameter of the tertiary γ' precipitates, the average distance to the centroid of the tertiary precipitate (ideally where nucleation begins) is approximately 107 nm.

[INSERT FIGURE 9 HERE]

Interestingly, the distribution also quantitatively captures several effects within the microstructure. First, the low occurrence of tertiary precipitates within 50 nm of the secondary precipitates (~8%) reflects that there is a zone around the secondary precipitates in which tertiary precipitates do not grow. This may result from the segregation of elements within the vicinity of the boundary [6, 10]. The width of this zone has important implications for Ni-based superalloys, because the spatial distribution of γ' precipitates impacts the overall mechanical properties.

Second, the highest or extreme value of the nearest neighbor distance (306 nm) may indicate the spacing of the secondary γ' precipitates. That is, there are no tertiary γ' precipitates greater than this distance because within a certain distance from the nearest secondary precipitate (~612 nm) the chemical composition is adequate for another secondary γ' precipitate to form. In this respect, the extreme value statistics of the nearest neighbor distances can give some insight into the maximum spacing of secondary γ' precipitates. In previous work, the distances between precipitates have been calculated using the equivalent diameter of the precipitates. Clearly, considering the tortuous morphology of the secondary γ' precipitates, the present technique for measuring nearest neighbor distances provides a much more accurate estimation of these distances, as well.

The ability to gather statistical information on both secondary and tertiary precipitates provides a great tool for the modeling community that has relied heavily on limited analysis of small particle populations. This has been driven by the labor-intensive manual techniques used to segment images with difficult intensity gradients across particle boundaries. The future of characterizing γ' precipitates in Ni-based superalloys relies not only on better techniques for imaging, but also better techniques for segmenting large numbers of γ' precipitates in an automated manner.

Conclusions

In this work, we discuss a computational methodology for automated detection of secondary and tertiary γ' precipitates in energy filtered transmission electron microscopy (EFTEM) images. Several important parameters for the automated region growing technique were investigated using a combination of visual inspection and intensity information from the EFTEM images. These parameters were related to the method used for calculating the stopping criterion, the local density weighting function, and the seed point selection method. After optimizing these parameters, the microstructural statistics obtained from the γ' precipitates segmented with the automated technique were compared with the same precipitates segmented manually. On average, the results show that the precipitate area (equivalent diameter) obtained using the automated technique is approximately 14% (7%) lower than that of the same precipitates segmented manually. The automated region growing technique presented here is suitable for detecting secondary and tertiary γ' precipitates of complex morphology and varying intensity contrast in a reproducible manner.

This technique was then used to segment the secondary and tertiary γ' precipitates from EFTEM images of a single crystal nickel-based superalloy that was slow cooled after aging for 200 hours. The segmented precipitates were used to calculate average/extreme microstructural statistics for this processing condition. In addition to calculating the distribution of tertiary precipitate equivalent diameters, the distribution of distances from 656 tertiary precipitates to the nearest secondary precipitates was calculated. The extreme values of the distribution shows that the

majority of tertiary γ' precipitates are located greater than 50 nm and less than 300 nm from the secondary γ' precipitate surfaces for this processing condition. The significance of this technique is its ability to automate segmentation of precipitates in a reproducible manner for acquiring microstructure statistics that relate to both processing and properties.

References

[1] Reed R.C., *The Superalloys Fundamentals and Applications*, (Cambridge, UK, Cambridge University Press, 2006).

[2] Telesman J., Kantzos P., Gayda J., Bonacuse PJ, Prescenzi A., Superalloys 2004, Warrandale PA, TMS Publications (2004), p.215.

[3] Stoloff N.S., Superalloys II, New York, John Wiley (1987) p. 61.

[4] Sondhi SK., Dyson BF, and McLean, Acta Materialia, Vol 52 (2000) p. 1761.

[5] Fahrmann M., Hermann W., Fahrmann E., BoegliA., Pollock TM., and Sockel HG., Mater. Sci and Eng., A271 (1991) p. 122.

[6] Tiley J., Viswanathan GB., Srinivasan R., Banerjee R., Dimiduk DM, and Fraser HL., Acta Materialia, Vol 57 (2009) p. 2538-2549.

[7] Tiley J., Searles T., Lee S., Kar S., Banerjee R., Russ J.C., Fraser H.L., Mat. Science and Eng A, 372 (2004) p. 191-198.

[8] Collins P.C., Welk B., Searles T., Tiley J., Russ J.C., Fraser H.L., Mat. Science and Eng A, 508 (2009) p. 174-182.

[9] Viswanathan G.B., Sarosi P.M., Henry M.F., Whitis D.D., Milligan W.W., and Mills M.J., Acta Materialia 53 (2005) p. 3041.

[10] Sarosi P.M., Viswanathan G.B., Whitis D.D., Mills M.J., Ultramicroscopy 103 (2003) p. 83.

[11] Littles Jr. J.W., Pettie R.G., Schirra J.J., Cowles B.A., Holmes R.A., Russ S.M., Materials damage prognosis, Warrendale PA, TMS Publications (2005) p. 23.

[12] Srinivasan R., Banerjee R., Hwang J.Y., Viswanathan G.B., Tiley J., Dimiduk D.M., Fraser H.L., Physical Review Letters 102 (2009) 086101.

[13] Russ, J.C., *The Image Processing Handbook*, 5th Edition (Boca Raton, FL, CRC Press, 2007).

[14] Gonzalez, R.C., Woods, R.E., *Digital Image Processing*, 2nd Edition (Upper Saddle River, NJ, Prentice-Hall, 2002).

[15] Simmons, J.P., Chuang, P., Comer, M., Spowart, J.E., Uchic, M.D., De Graef, M., MSMSE 17 (2009) 025002.

[16] Law, T.S., Heng, P.A., Medical Imaging 2000: Image Processing, Kenneth Hanson (Editor), Proceedings of SPIE, 3979 (2000) 906-916.

[17] Pohle, R., Toennies, K.D., Medical Imaging 2001: Image Processing, Milan Sonka, Kenneth Hanson (Editor), Proceedings of SPIE, 4322 (2001) 1337-1346.

[18] M. del Fresno, M. Vénere, A. Clausse, *Computerized Medical Imaging and Graphics*, 33 (2009) 369-376.

Table 1
The percent change in the area, perimeter, and equivalent diameter measurements for the secondary/tertiary γ' precipitates when compared to region growing unbiased by the weighting function (*m/c* = 3/1).

m	c	Secondary γ' Area Change	Tertiary γ' Area Change	Secondary γ' Perimeter Change	Tertiary γ' Perimeter Change
3	1	Segmentation is unbiased by local density weighting function			
3	2	0	+ 1%	-8 %	-17 %
3	3	0	+ 2%	-14 %	-26 %
3	4	- 1%	0	-27 %	-39 %
3	5	-1%	+ 1%	-28 %	-40 %
5	3	0	0	0	-2 %
5	5	0	0	-2 %	-6 %
5	7	0	0	-5 %	-14 %
5	9	0	+ 2%	-11 %	-25 %
5	11	-1%	0	-26 %	-39 %
7	5	0	0	0	0
7	9	0	0	0	-2 %
7	13	0	0	-2 %	-6 %
7	17	0	+ 1%	-7 %	-17 %
7	21	0	+ 1%	-17 %	-32 %

Figure 1

Images showing the variations in precipitate morphology for primary (1-8) and secondary (9-16) γ’ precipitates.

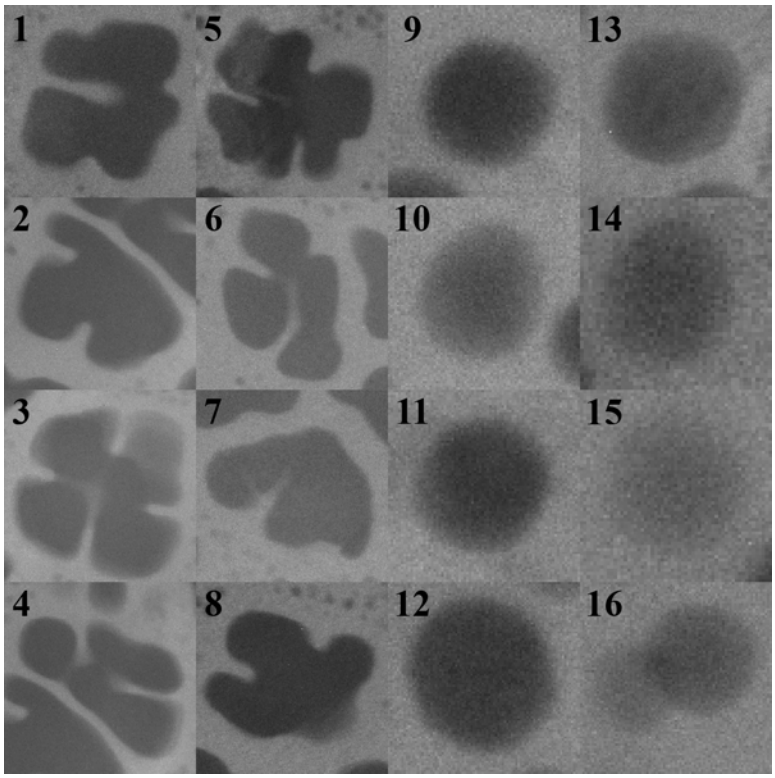

Figure 2

(a) Plot showing the region size as a function of the stopping threshold parameter. (b) Plot showing the mean intensity for the region, the area just outside the region, and the intensity difference between the two areas as a function of the stopping threshold parameter. The arrow and image correspond to the region with the maximum intensity difference, which is used for the automated region growing stopping criterion.

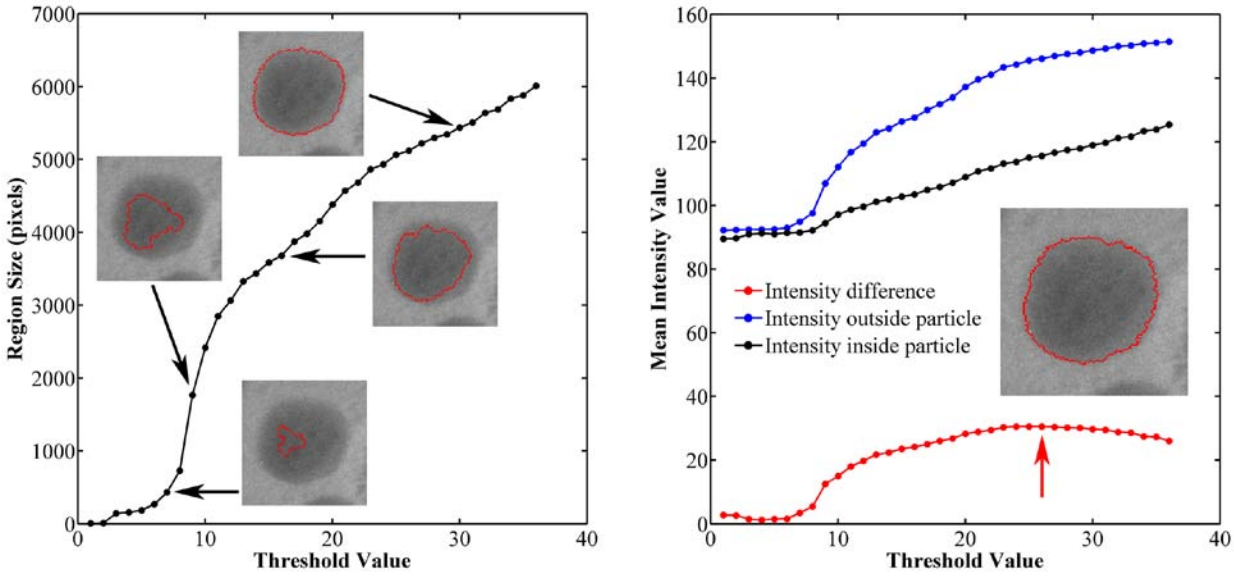

(a) (b)

Figure 3

Images showing how the width of the border used in the mean intensity calculation and the choice of method for calculating the region mean intensity influences the segmentation of a secondary γ' precipitate. The notation refers to the border width (*i.e.*, the numbers 2 and 7 are the border width in pixels) and the two methods for calculating the region mean intensity, *i.e.*, (i) using pixels from the entire region or (ii) just using pixels from the outer border of the region (using the same aforementioned border width).

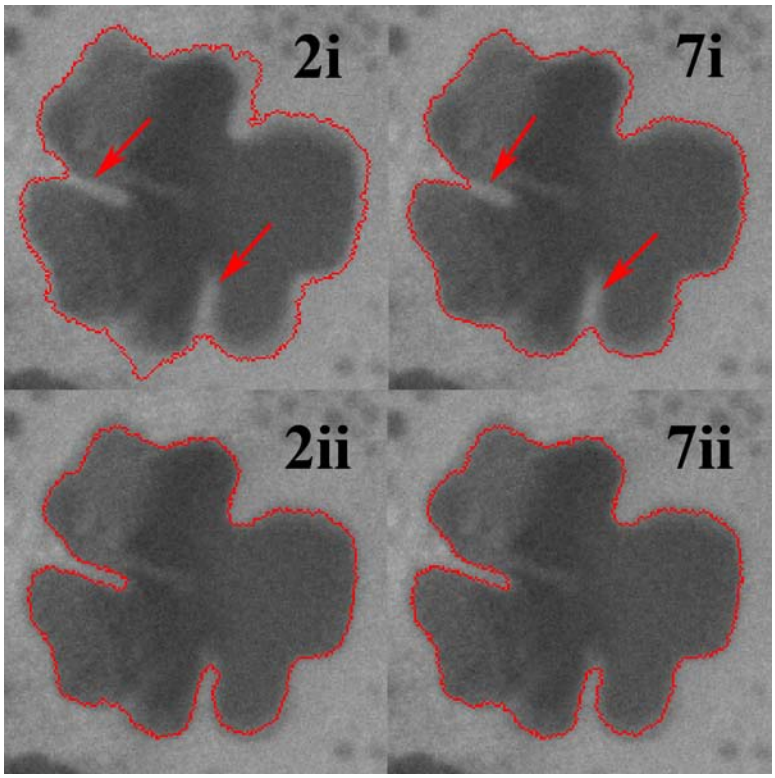

Figure 4
Images showing the influence of the local density weighting function parameters on the segmentation of a tertiary γ' precipitate. The parameters *c* and *m* refer to a normalization constant *c* for the weighting function and the size of the local neighborhood (*m* x *m*), respectively.

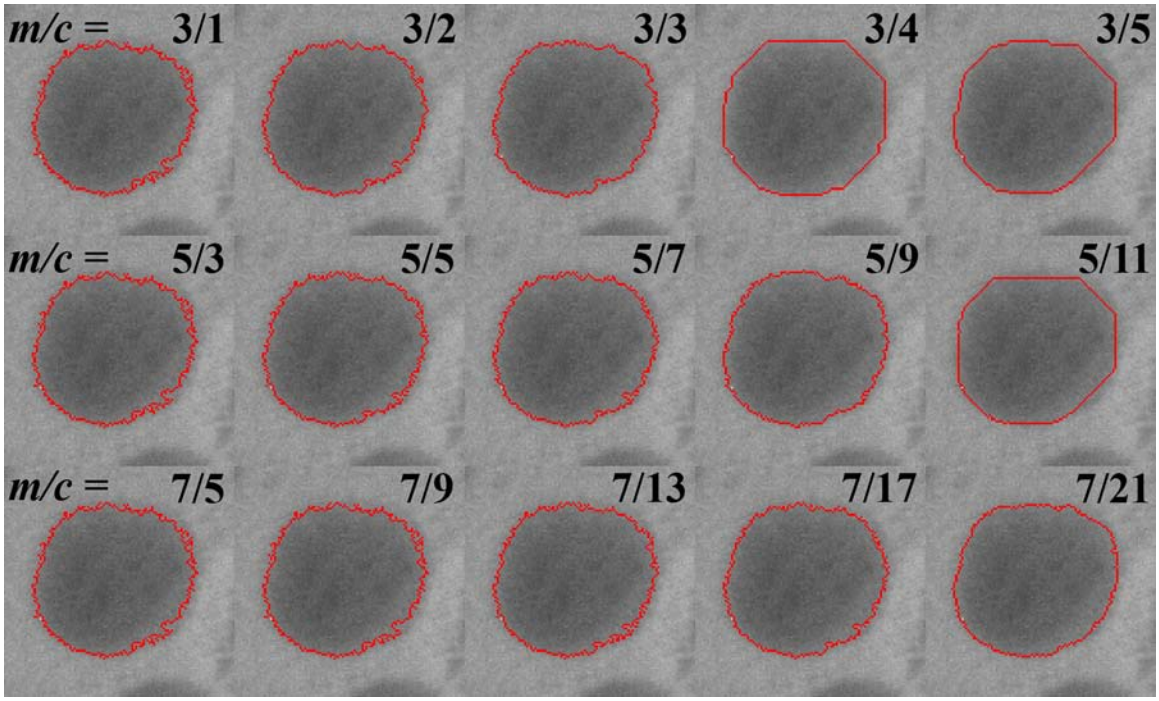

Figure 5

Images showing the intensity image of the tertiary γ' precipitate along with the 250 random seed point locations. The colors correspond to the size of the segmented region relative to the region grown using the lowest intensity (darkest) seed point.

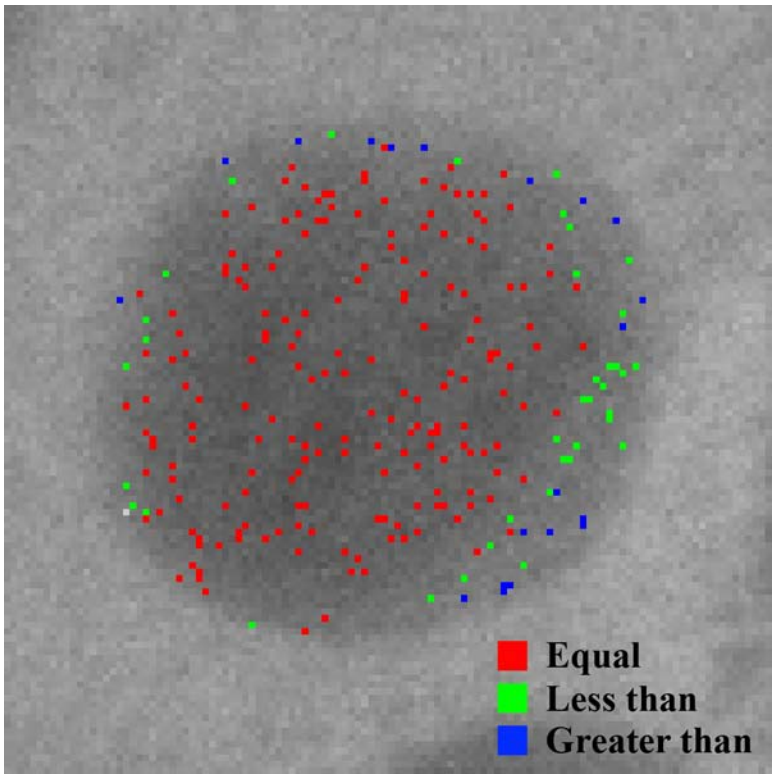

Figure 6

Images showing the segmentation of the region growing technique with the optimum parameters (border width of 7 pixels, method 'ii', *m/c* = 5/9) for variations in precipitate morphology for primary (1-8) and secondary (9-16) γ' precipitates.

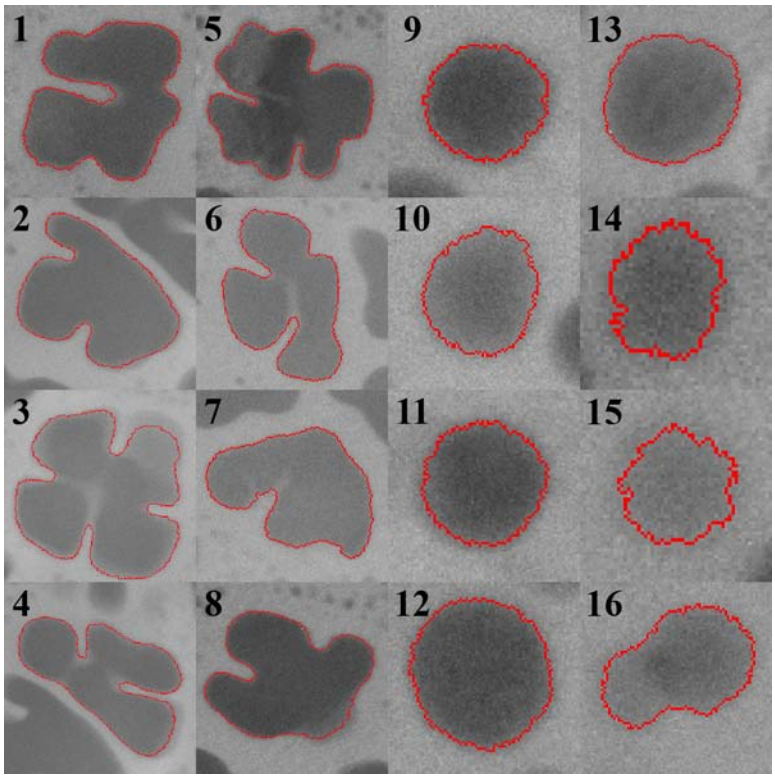

Figure 7

Plot comparing the area of 50 manually segmented precipitates versus the area of these same precipitates segmented with the region growing algorithm. The images show examples of some of the secondary and tertiary precipitates with the perimeter of the manually and automated precipitates shown in blue and red, respectively.

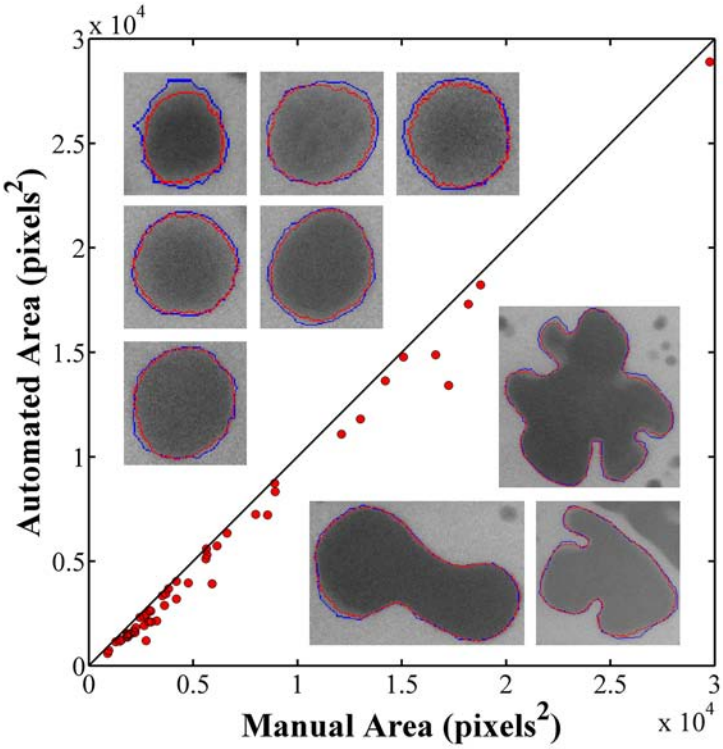

Figure 8

(a) Intensity image with segmented secondary (blue) and tertiary (red) γ' precipitates using the automated technique. (b) Histogram assembled from multiple EFTEM images, which shows the distribution of equivalent diameters (nm) for 656 tertiary γ' precipitates. The average equivalent diameter is 26 nm ± 13 nm.

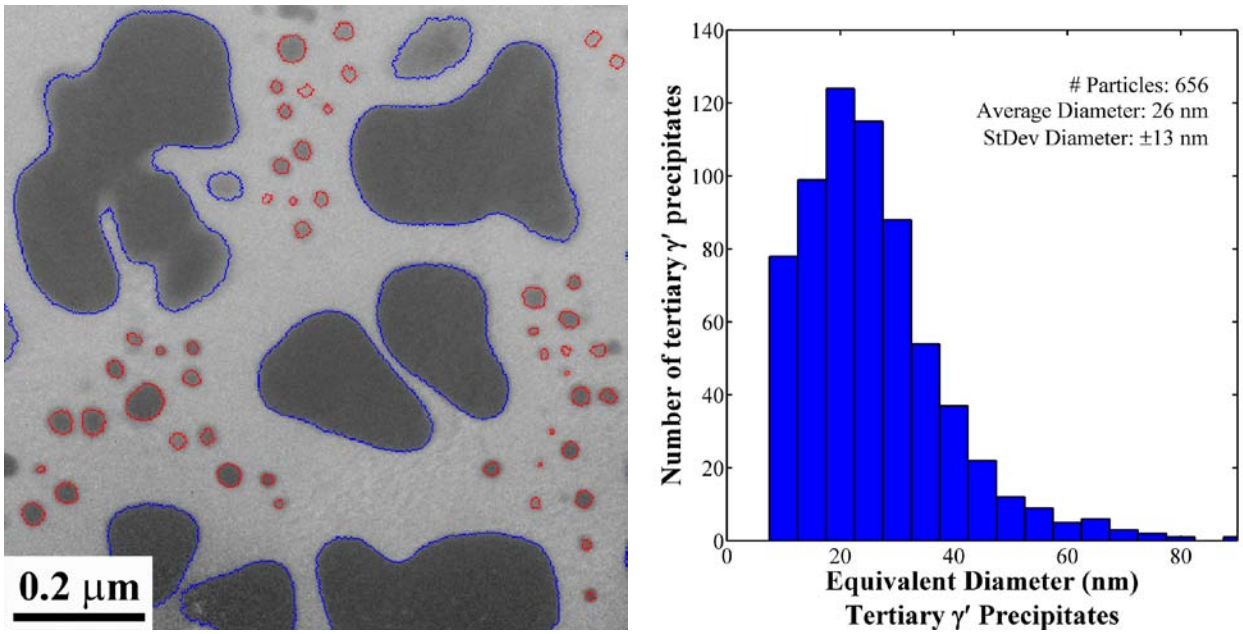

(a) (b)

Figure 8

Histogram showing the distribution of nearest neighbor distances (nm) for 656 tertiary γ' precipitates to the nearest secondary γ' precipitates. The average nearest neighbor distance is 94 nm ± 39 nm.